

A generalized mass transfer law unifying various particle transport mechanisms in dilute dispersions

Abhijit Guha

Received: 3 February 2006 / Accepted: 14 January 2008 / Published online: 12 February 2008
© Springer-Verlag 2008

Abstract A generalized mass transfer law for dilute dispersion of particles (or droplets) of any sizes suspended in a fluid has been described, which can be applied to turbulent or laminar flow. The generalized law reduces to the Fick's law of diffusion in the limit of very small particles. Thus the study shows how the well-known and much-used Fick's law of diffusion fits into the broader context of particle transport. The general expression for particle flux comprises a diffusive flux due to Brownian motion and turbulent fluctuation, a diffusive flux due to temperature gradient (thermophoresis plus stressphoresis) and a convective flux that arises primarily due to the interaction of particle inertia and the inhomogeneity of the fluid turbulence field (turbophoresis). Shear-induced lift force, electrical force, gravity, etc. also contribute to the convective flux. The present study includes the effects of surface roughness, and the calculations show that the presence of small surface roughness even in the hydraulically smooth regime significantly enhances deposition especially of small particles. Thermophoresis can have equally strong effects, even with a modest temperature difference between the wall and the bulk fluid. For particles of the intermediate size range, turbophoresis, thermophoresis and roughness are all important contributors to the overall deposition rate. The paper includes a parametric study of the effects of electrostatic forces due to mirror charging. The present work provides a unified framework to determine the combined effect of various particle transport mechanisms on mass transfer rate and the

inclusion of other mechanisms not considered in this paper is possible.

List of symbols

c	concentration
D_B	Brownian diffusivity
D_t	turbulent diffusivity
D_T	coefficient of temperature-gradient-driven diffusion (Eq. 14)
E	field strength of externally applied electric field
F_S	shear induced lift force (per unit mass of a particle)
G_E	electrical force (per unit mass of a particle)
J	flux of particles
k	Boltzmann constant
Kn	Knudsen number
k_s	effective roughness height
m	mass of a particle ($m = \frac{4}{3}\pi r^3 \rho_p^0$)
p	pressure
q	total charge on a particle
r	radius of particles
T	temperature
u_*	frictional velocity
V	velocity
V_{dep}	deposition velocity
$V_{\text{p,turbo}}$	turbophoretic velocity of particle (Eq. 20)
x	co-ordinate along the flow direction
y	co-ordinate perpendicular to the wall
ΔT	temperature difference between wall and $y^+ = 200$
\Re	ratio of particle and fluid mean-square velocities
ξ	non-dimensional number used to specify electrical charge on a particle

A. Guha (✉)
Aerospace Engineering Department, University of Bristol,
University Walk, Bristol BS8 1TR, UK
e-mail: a.guha@bristol.ac.uk

ε	eddy viscosity
η	thermophoretic force coefficient
λ	thermal conductivity
μ	viscosity of fluid
ν	kinematic viscosity of fluid
ρ	density
ρ_p	partial density of particles
τ	relaxation time of particles

Superscripts

c	convective
+	non-dimensional
'	fluctuating quantities
($\bar{\quad}$)	mean quantities

Subscripts

f	fluid
p	particle
x	along x -direction
y	along y -direction

1 Introduction

Mass transfer can be effected in various ways. It may be due to Brownian diffusion or turbulent diffusion of particles (or droplets) suspended in a flowing fluid, which depends on the gradient of particle concentration. A diffusive mass flux may also arise due to a gradient in temperature (thermophoresis). A convective mass flux may arise due to various reasons: the inability of inertial particles to follow curved fluid streamlines (inertial impaction) or to quickly respond to changes in fluid speed, the action of body forces such as gravity (gravitational settling), electrical forces and magnetic forces, the effects of shear-induced lift force, and the interaction of particle inertia and the inhomogeneity of the fluid turbulence field (turbophoresis). Mass transfer rate is also affected by surface conditions such as the effective heights of roughness elements. In this paper, a generalized mass transfer law is described, which shows that the most commonly used mass transfer law, the Fick's law of diffusion, is valid only in the limit of small particles. The paper provides a unified framework to treat various particle transport mechanisms. Example calculations are included to show how particular models for various transport mechanisms can be incorporated in this general framework (the users can easily replace these example models with more accurate versions if desired).

We have discussed the physical processes by which solid particles (or liquid droplets) suspended in a fluid are transported to and deposited on solid walls. Measuring, predicting and understanding the rate of deposition are

both scientifically interesting and of engineering importance, and consequently these have been the subject-matter of an extremely large number of studies. Some or all of the described physical processes are responsible, for example, in deposition of drugs and aerosols in the respiratory tract (medical science and engineering), fouling of mechanical equipments such as heat exchangers, the deposition of particles in gas turbines and droplets in steam turbines (mechanical engineering), dispersal of pollutants in the atmosphere and determining indoor air quality (environmental science), transport of chemical aerosols, etc. The presented theory covers both laminar and turbulent flow of the fluid. So the equations, for example, can describe macroscopic transport due to a convective velocity set up in the laminar flow. Natural convection may also contribute in setting up the fluid flow field. Some of the particle transport mechanisms are also operative in a static fluid (for example, gravitational settling, Brownian diffusion, etc.). Only dilute mixtures, i.e., when the volume fraction of the dispersed phase is low, are considered here. The particles or droplets are therefore assumed not to interact with each other and to exhibit one-way coupling (i.e., the particle motion depends on the fluid flow field but not vice versa). This paper attempts to bring the modern developments in the theory of deposition to the domain of mass transfer so that cross-fertilization is effected and to describe Fick's law in the broader context of particle transport. The emphasis is given here on the physical understanding of the particle transport mechanisms.

Most textbooks on mass transfer [12, 28] show that the flux of small particles in a turbulent boundary layer can be calculated by integrating a modified Fick's law of diffusion,

$$J = -(D_B + D_t) \frac{dc}{dy} \quad (1)$$

where D_B is the Brownian diffusivity, D_t is the turbulent diffusivity which varies with position, y is the perpendicular distance from the wall, and dc/dy is the concentration gradient. D_B is given by the Einstein equation incorporating the Cunningham correction [11] for rarefied gas effects ($C_C = 1 + 2.7 \text{ Kn}$),

$$D_B = \frac{kT}{6\pi\mu r} C_C \quad (2)$$

where k is the Boltzmann constant, T is the absolute temperature, μ is the dynamic viscosity and Kn is the Knudsen number defined by $\text{Kn} \equiv l/2r$ where l is the mean free path of the surrounding gas and r is the radius of a particle.

Equation (2) shows that D_B decreases with increasing r . Equation (1) therefore predicts that the mass flux of particles decreases continuously with increasing particle size.

Experiments, on the other hand, predict a much more complicated variation, as shown in Fig. 1.

Usually the results of deposition experiments or calculations are presented as curves of non-dimensional deposition velocity versus non-dimensional particle relaxation time. The deposition velocity, V_{dep} , is the particle mass transfer rate on the wall, J_{wall} , normalized by the mean or bulk density of particles (mass of particles per unit volume) ρ_{pm} in the flow

$$V_{dep} = J_{wall}/\rho_{pm} \tag{3}$$

The particle relaxation time, τ , is a measure of particle inertia and denotes the time scale with which any slip velocity between the particles and the fluid is equilibrated. The physical significance of relaxation time has been explained by Ref. [2, 20, 21]. In the Stokes drag regime τ is given by,

$$\tau = 2\rho_p^0 r^2 / 9\mu \tag{4a}$$

where ρ_p^0 is the density of pure particulate material.

We have plotted the results with this definition of relaxation time to be consistent with other works in the field. However, in the numerical calculations we have corrected the relaxation time to account for the slip velocity for large particles and rarefied gas effects for very small particles. The rarefied gas effects can be modelled by Cunningham correction factor used in Eq. (2), while the effects of large slip Reynolds number is modelled according to Ref. [36]. The general expression for the inertial relaxation time τ_1 is then given by

$$\tau_I = \tau \frac{24}{Re C_D} C_C \tag{4b}$$

where Re is the slip Reynolds number defined as ($Re = 2r\Delta V/\nu$), where ΔV is the slip velocity between the two phases and ν is the kinematic viscosity of the fluid. C_D is the particle drag coefficient and is a function of Re , empirical values of C_D are given by Morsi and Alexander in several piecewise ranges of slip Reynolds number. The method of analysis is not dependent on the form of Eq. (4b), however, and, if desired, any other suitable expressions can easily be incorporated [9, 25] for alternative expressions, and also for values of C_D for non-spherical particles].

V_{dep} and τ are made dimensionless with the aid of the fluid friction velocity u_*

$$V_{dep}^+ \equiv V_{dep}/u_* \tag{5}$$

$$\tau^+ \equiv \frac{\tau u_*^2}{\nu} = \frac{2}{9} \left(\frac{\rho_p^0}{\rho_f} \right) \frac{r^2 u_*^2}{\nu^2}$$

where ρ_f is the fluid density.

Figure 1 shows a typical, schematic plot of V_{dep}^+ versus τ^+ as obtained by experiments in fully-developed vertical pipe flow. There are many references giving experimental measurements of the deposition velocity. The experimental data of [18, 32, 56], and the compilation of McCoy and Hanratty [34] show considerable scatter, but all data show the basic characteristics shown in Fig. 1. Three distinct regimes can be identified on the S-shaped curves. The borders between the three regimes are not sharp, as one effect gradually merges into another, and depend on flow conditions. In regime 1, as τ^+ increases, the deposition velocity *decreases*. This is the so-called “turbulent diffusion regime”. It is only for small particles in regime 1 that the experimentally measured mass transfer rates can be explained on the basis of Eq. (1), the turbulent version of the Fick’s law of diffusion. The next zone is the so-called “turbulent diffusion—eddy impaction regime”. The striking feature of this regime is that the deposition velocity *increases* by three to four orders of magnitude. Separate models representing additional mechanisms of deposition had to be developed in order to explain this behaviour of deposition velocity. One of the most used calculation methods is called the “free flight” or “stop distance” model (e.g., [1, 13, 18, 39, 57]. Friedlander and Johnstone’s work is a landmark paper in the field of deposition calculations because it was the first to offer a theoretical calculation method for the observed large increase in deposition velocity in regime 2 of Fig. 1.

In all of the various “free flight” models it is assumed that particles diffuse to within one “stop distance”, s , from the wall, at which point they make a “free flight” to the

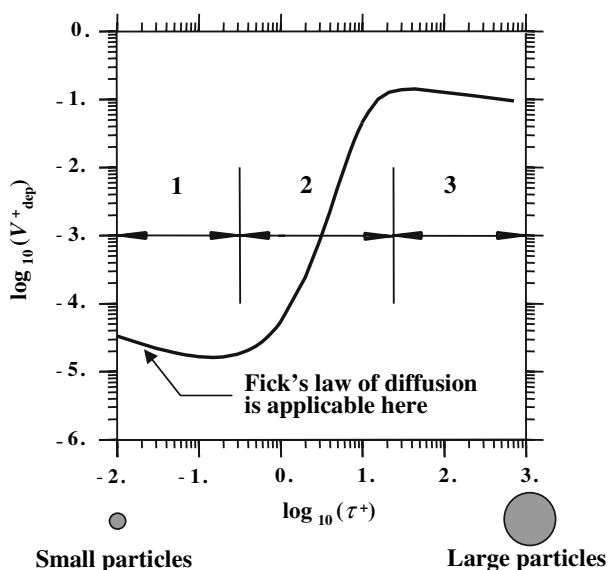


Fig. 1 A typical variation in measured deposition rate with particle relaxation time. Regime 1: Turbulent diffusion, Regime 2: Turbulent diffusion—eddy impaction, Regime 3: Particle inertia moderated

wall. The main difference between different models of this type lies in prescribing the free flight velocity, v_{ff} . Friedlander and Johnstone [18] assumed $v_{ff} = 0.9u_*$, a value close to the fluid r.m.s. velocity in the outer layer of a turbulent boundary layer. Their model agrees well with experiments in pipe flows. Davies [13] made an apparently more plausible assumption that the free flight velocity is the same as the *local* r.m.s. velocity of the *fluid*, but his computed deposition velocities were lower by some two orders of magnitude than the experimentally observed values. Liu and Ilori [33] improved the prediction of this model by prescribing, rather arbitrarily, a particle diffusivity which was different from the commonly used eddy momentum diffusivity). Beal [1] gave another variation of the stop distance model.

It may be seen that these models, while significantly contributing to the development of our current understanding of the deposition process, are physically not very satisfactory. The “stop distance” models predict a *monotonic* rise in stop distance (which may exceed the buffer layer thickness of a turbulent boundary layer for larger particles, since $s^+ \sim \tau^+$), and consequently predict a monotonic increase in deposition velocity with increasing τ^+ . Experiments, however, show a third regime of deposition, usually termed “particle inertia moderated regime”, in which the deposition velocity *decreases* with further increase in τ^+ (see Fig. 1). Stop distance models cannot be used here, and new theories (e.g., [46]) need to be applied.

Thus, even for the apparently simple case of turbulent deposition in a fully developed pipe flow, separate theories had to be applied for each of the deposition regimes. Although it is possible, with proper tuning of the models (e.g., by prescribing the free flight velocity), to partially reproduce the experimental results for fully developed pipe flow, the theories cannot be extrapolated to two or three dimensional flow situations with any great confidence because of their piecemeal nature and of the required empirical tuning. Additionally, when other effects such as thermophoresis or electrostatic interaction are present, the stop distance models would need postulations such as that the deposition velocities due to various mechanisms calculated separately can be simply added (linear superposition).

Whereas the genre of “free flight” models tried to capture the physics of deposition by solving the particle continuity equation alone, in the past 15 or so years, Eulerian computational methods of deposition have been developed that solve *both* particle continuity and momentum equations [22, 26]. These models show that the interaction of particle inertia and the inhomogeneity of fluid turbulent flow field (in the boundary layer close to

a solid surface) gives rise to a new mechanism of particle transport called turbophoresis [6, 43]. Turbophoresis (where particle transport is caused by gradients in fluctuating velocities) is a separate effect and must be treated as such, it cannot be properly reproduced by any tuning of the theoretical model for diffusion (that is driven by the gradient of concentration). Turbophoresis is not a small correction to the Fick’s law of diffusion, indeed it is shown by Ref. [22] that it is the primary mechanism operative in regimes 2 and 3 of Fig. 1). It is further shown that, for large particles, the momentum equation alone can provide nearly accurate estimates of the deposition velocity; the absence of the use of the particle momentum equation in the “stop distance” models is therefore their major weakness. Theoretical treatments on motion of particles in turbulent flow, including kinetic approaches, are given by Refs. [40, 42, 44, 45, 47, 51, 58] among others. Other aspects of particle dynamics are given by Ref. [13, 52]. Crowe [10] has given a review of various computational fluid dynamics (CFD) techniques used for two-phase flows.

A large number of studies have adopted the alternative approach of particle tracking in a Lagrangian framework (again assuming dilute mixtures). In these methods, the momentum equation for the particle is written and then integrated with respect to time along the *particle path line*. For example, Ref. [27] calculated the deposition of particles in a simulated turbulent fluid field; Refs. [5, 38] computed the motion of particles where the fluid motion was determined by direct numerical simulation (DNS) of the Navier–Stokes equations; Ref. [55] solved the fluid velocity field by large eddy simulation (LES); and the calculations of Ref. [15, 16] were based on the sublayer approach originally proposed by Ref. [8]. The paper by Kallio and Reeks [27] is important in terms of deposition calculations, because (despite its inability to capture regime 1 in Fig. 1 as a result of ignoring Brownian movement) it showed that a simple stochastic theory could predict the general behaviour of particle deposition in regimes 2 and 3 of Fig. 1.

There are several attractions of Lagrangian methods: the form of the particle momentum equation is simple and direct, the method can be applied to complex flow geometries, surface–particle interactions such as rebound can be modelled easily, and the numerical coding requirement is relatively modest. The stochastic trajectory calculations are illustrative and important for physical understanding. However, Lagrangian computations typically involve the determination of trajectories of a very large number of particles (to establish statistically meaningful ensemble average quantities) and may be too time-consuming to be

effective as a practical calculation method or as a design tool, especially for small particles. It is also difficult to calculate concentration profile in this method. Moreover, all practical CFD computations for a single-phase fluid in complex geometries are performed in the Eulerian framework. Hence, it is profitable to solve the particle equations in the same way for easy integration with the established CFD codes for the primary fluid.

Guha [22] has derived, from the fundamental conservation equations of mass and momentum for the particles, a unified Eulerian advection–diffusion theory in which turbophoresis and all other particle transport mechanisms arise naturally. It has been shown that the prediction of deposition velocity from this Eulerian theory is at least as accurate as those from the state-of-the-art Lagrangian calculations, including DNS studies, but the Eulerian computation is much faster (and the inclusion of Brownian diffusion is simple). Submitted in 1995 and published in 1997, forty years after the landmark paper by Ref. [18], the paper of Guha [22] thus represents considerable progress in the physical understanding of the deposition process.

2 Formulation of the unified advection–diffusion theory

2.1 Mathematical foundation

The proper way of deriving the equations for particle transport is to write the particle continuity and the momentum conservation equations, split the different flow quantities into their respective mean and fluctuating components, and then perform Reynolds averaging. If the fluid flow field is known, the Reynolds averaged particle conservation equations would specify the motion of the particles.

One of the major reasons why the Fick’s law of diffusion does not work for larger particles is that it neglects a mechanism, operative in inhomogeneous turbulent flow that assumes dominance for large particle relaxation times. Just like particles move against the concentration gradient, particles also move against a gradient in turbulence intensity. The latter phenomenon is called turbophoresis which may be qualitatively understood by analogy with concentration-gradient-driven diffusion.

Suppose, there is a non-uniform distribution of particles in homogenous turbulence. Small particles almost faithfully follow the fluid eddies. At any particular location, the probability of a particular particle being transported by a fluid eddy to the left is the same as that to the right. However, because of the non-uniform

concentration of particles, the number of particles that arrive at a particular cross-sectional plane from regions of higher concentration is greater than the number of particles that arrive at the same cross-sectional plane from regions of lower concentration travelling in the opposite direction (just because there are more particles in the former region than the latter). Consequently there is a net flux of particles from regions of higher concentration to lower concentration. This process is modelled by the Fick’s law of diffusion.

Now consider a uniform concentration of particles in an inhomogenous turbulent flow in which there is a gradient of turbulence intensity in the carrier fluid. The particles are assumed large to have considerable inertia so that they may slip through the containing eddy. (Later, in Sect. 5.2, the corresponding quantitative argument is given as to why turbophoresis is not important for very small particles even in the presence of a gradient in fluid turbulence intensity.) At a particular location, the probability of a fluid eddy throwing a particle towards the left is the same as that of a fluid eddy throwing a particle towards the right. Consider an imaginary cross-sectional plane between a region of high turbulence intensity and that of low intensity. The probability of a particle being thrown from a region of low turbulence intensity and reaching the particular cross-sectional plane is lower than the probability of a particle being thrown from a region of high turbulence intensity and reaching the plane. There would thus be a net flux of particles through the plane in a direction of high to low turbulence intensity. This constitutes the physical picture of turbophoresis.

In order to formulate a unified theory of turbulent deposition one, therefore, has to combine concentration-gradient-driven deposition (Fick’s law) with turbophoresis. It turns out that such a uniform description automatically arises from the basic conservation equations of the fluid-particle system. We follow the approach of Ramshaw [41] to describe the motion of a particle cloud in a flowing fluid. The particles are assumed to constitute a hypothetical ideal gas whose partial pressure p_p is given by

$$p_p = (k/m)\rho_p T \quad (6)$$

where m is the mass of an individual particle and ρ_p is the partial density. It is assumed, while writing Eq. (6), that the particles are in local thermal equilibrium with the surrounding fluid. This equilibrium is brought about by their collisions with the fluid molecules, the particles themselves rarely collide with each other. If n is the number of particles per unit volume of the mixture, then ρ_p is given by

$$\rho_p = nm \quad (7)$$

ρ_p is the same as particle concentration, c , used in Eq. (1). The motion of the hypothetical ideal gas consisting of the particles is governed by the continuity and the momentum equations of fluid dynamics. For simplicity, we assume that the radius of the pipe is large so that the effects of the curvature can be neglected and the governing equations can be profitably written in the Cartesian coordinate. In the steady state, the equations of motion are

$$\nabla \cdot (\rho_p \mathbf{V}_p) = 0 \tag{8}$$

$$\rho_p (\mathbf{V}_p \cdot \nabla) \mathbf{V}_p = -\nabla p_p + \rho_p \mathbf{F} + \rho_p \mathbf{G} \tag{9}$$

where the vector \mathbf{V}_p represents the mean velocity of the particles, on which is superposed a random thermal velocity that gives rise to the partial pressure p_p . As a result of the equipartition of energy, the rms thermal velocity of the particles is much less than that of the fluid molecules. \mathbf{F} is the mean force per unit mass on the particles due to the fluid and \mathbf{G} is the total external force per unit mass (e.g., gravitational, electromagnetic) on the particles. \mathbf{F} is given by,

$$\mathbf{F} = (\mathbf{V}_f - \mathbf{V}_p)/\tau_1 - (\eta/m)\nabla \ln T - \left(1/\rho_p^o\right)\nabla p + \mathbf{F}_v + \mathbf{F}_B + \mathbf{F}_S \tag{10}$$

where, \mathbf{V}_f is the fluid velocity, ρ_p^o is the mass density of the pure particulate material, p is the true pressure of the fluid-particle system, η is the thermophoretic force coefficient. \mathbf{F}_v , \mathbf{F}_B and \mathbf{F}_S are the virtual mass force, the Basset-Boussinesq force and the shear-induced lift force, respectively. The term containing ∇p is the source of the buoyant force on a particle in a stationary fluid in a gravitational field. This term and \mathbf{F}_v and \mathbf{F}_B are usually small (because of the high material density, ρ_p^o , of the particles) compared with the first term on the RHS of Eq. (10) which represents the steady state drag force. In the present study they are not included. The thermophoretic force may become appreciable for small particles if the temperature gradient is high (as is the case for internally cooled gas turbine blades) and is retained in the present analysis. An equation for the thermophoretic force coefficient, η , is given by Talbot et al. [53],

$$\eta = \frac{2.34(6\pi\mu vr)(\lambda_r + 4.36Kn)}{(1 + 6.84Kn)(1 + 8.72Kn + 2\lambda_r)} \tag{11}$$

where, λ_r is the ratio of the thermal conductivity of the fluid, λ_f , and that of the particles, λ_p ($\lambda_r = \lambda_f/\lambda_p$).

Consider a two-dimensional flow field and decompose the instantaneous flow parameters into their mean and fluctuating parts

$$\begin{aligned} V_{fx} &= \bar{V}_{fx} + V'_{fx} \\ V_{fy} &= \bar{V}_{fy} + V'_{fy} \\ V_{px} &= \bar{V}_{px} + V'_{px} \\ V_{py} &= \bar{V}_{py} + V'_{py} \\ \rho_p &= \bar{\rho}_p + \rho'_p \end{aligned} \tag{12}$$

where the suffix x represents the respective components along the x -coordinate which is along the flow direction and the suffix y represents the respective components in the direction perpendicular to the wall. The suffices f and p refer to the fluid and the particles, respectively. We now substitute Eq. (12) into Eqs. (8) and (9), and take time-mean of the resulting equations. The details of the procedure are given in Appendix 1.

2.2 Physical description

If the flux of particles in the y direction (which is perpendicular to the solid wall) is denoted by J , then the Reynolds averaging of the continuity equation (Eq. 8) for fully developed flow gives (see Appendix 1)

$$\partial J / \partial y = 0$$

where,

$$J = - (D_B + D_t) \frac{\partial \bar{\rho}_p}{\partial y} - D_T \bar{\rho}_p \frac{\partial \ln T}{\partial y} + \bar{\rho}_p \bar{V}_{py}^c \tag{13}$$

The coefficient of temperature-gradient-dependent diffusion, D_T , in Eq. (13) is given by

$$D_T = D_B(1 + \eta/kT). \tag{14}$$

Equation (14) shows that the thermal drift has a “stressphoretic” component and a thermophoretic component. Usually most references include the thermophoretic component only in their calculations. The “stressphoretic” component arises from the evaluation of ∇p_p in Eq. (9) with the help of Eq. (6).

Equation (13) is the generalized equation for particle flux. The particle convective velocity in the y -direction, \bar{V}_{py}^c , appearing in Eq. (13), has to be calculated from the particle momentum equation. The Reynolds-averaged particle momentum equations (Eq. 9) in the y and x directions, slightly simplified and specialized for fully developed vertical flow are (Appendix 1):

y-momentum:

Acceleration term	Viscous drag	Turbo-phoresis	Shear-induced lift	Electrical force
-------------------	--------------	----------------	--------------------	------------------

$$\bar{V}_{py}^c \frac{\partial \bar{V}_{py}^c}{\partial y} + \frac{\bar{V}_{py}^c}{\tau_1} = - \frac{\partial \bar{V}_{py}^{\prime 2}}{\partial y} + F_{Sy} + G_{Ey} \tag{15a}$$

x – momentum :

$$\bar{V}_{py}^c \frac{\partial \bar{V}_{px}}{\partial y} = \frac{1}{\tau_1} (\bar{V}_{fx} - \bar{V}_{px}) + \left(1 - \frac{\rho_f}{\rho_p^0} \right) g \tag{15b}$$

The second term in the LHS of Eq. (15a) is the steady state drag term simplified with the assumption $\bar{V}_{fy} = 0$; the full form is $-(\bar{V}_{fy} - \bar{V}_{py}^c)/\tau_1$. For vertically upwards flow, replace g by $-g$. Note that the x -momentum Eq. (15b) involves both \bar{V}_{px} and \bar{V}_{py}^c . The y -momentum Eq. (15a), on the other hand, is almost decoupled and depends on \bar{V}_{px} only through the shear-induced lift force, F_{Sy} . A study of Eqs. (15a) and (15b) also shows nicely how gravity affects the y -momentum equation through the lift force. The LHS of equation (15b) involves \bar{V}_{py}^c . As a result of this convective velocity in the y -direction, the direction of the lift force may remain unaltered [22] whether the flow is vertically downwards or upwards, and the influence of gravity on the deposition velocity is likely not to be serious in vertical flow. The turbulent fluctuations may alter the magnitudes of the time-mean values of the forces (such as the lift force); it is usually assumed in deposition calculations that such effects are small and the values of the forces as they would occur in the time-mean flow field are usually used.

In the general case, both Eqs. (15a) and (15b) must be solved simultaneously. Calculations show that the shear-induced lift force increases the deposition rate, particularly in the “eddy diffusion-impaction” regime. In this connection it should be noted that, in the literature, the Saffman lift force is usually used in deposition calculations. Saffman [48, 49] originally derived this expression of lift force for unbounded shear flow. Hence for deposition calculations the equation for shear-induced lift should include modifications due to the proximity of a solid wall and finite Reynolds number. The effect of the lift force, F_{Sy} , is not considered in the remainder of this paper. With these provisos, the particle convective velocity in the y -direction, \bar{V}_{py}^c , can be calculated from

$$\bar{V}_{py}^c \frac{d}{dy} (\bar{V}_{py}^c) + \frac{\bar{V}_{py}^c}{\tau_1} = - \frac{d}{dy} \left(\bar{V}_{py}^{\prime 2} \right) + G_{Ey}. \tag{15c}$$

A charged aerosol will be subjected to electrical forces. If there is an externally applied electric field of strength E and

the total charge carried by a particle is q , then the Coulomb force due to the imposed field is qE . A charged aerosol near a solid wall also experiences an electrostatic force due to induced charges on the wall (mirror charging). The easiest way to find the force is the method of images [37]. If the wall is conducting then it is an equipotential line and the electrostatic force on a particle at distance y from the wall can be found by placing an opposite charge (image) at $-y$. The electrostatic force due to mirror charging is, in this case, of an attractive nature (i.e., acts towards the wall assisting deposition) and its magnitude per unit mass of the particle can be calculated by the Coulomb’s law. The total electrical force (per unit mass of a particle) in the y -direction is then given by

$$G_{Ey} = \frac{qE}{m} - \frac{3q^2}{64\pi^2 \epsilon_0 \rho_p^0 r^3 y^2}. \tag{16}$$

where, ϵ_0 is the electric permittivity of vacuum (or air). An expression for the maximum charging of a particle q_{max} is given by Hesketh [24], $q_{max} = 2000 \times (1.6 \times 10^{-19})(r/10^{-6})^2$ Coulomb. In order to make a parametric investigation of the effects of mirror charging on the particle motion we have expressed $q = \xi q_{max}$. There are other terms such as dielectrophoretic force, dipole-dipole interaction, interaction due to neighbouring particles, which are usually small and are not considered in this paper. In numerical illustrations it is assumed that there is no external field, i.e., $E = 0$; it is straight-forward to include this term.

The equation set (13)–(15) is almost exact and should work well if one could find an accurate expression for the particle rms velocity as a function of the wall coordinate. The variation of fluid rms velocity as a function of wall coordinate has been measured and is documented (Sect. 3). We, therefore, relate the particle mean square velocity to the fluid mean square velocity through a parameter \mathfrak{R} which is defined as the ratio of the two

$$\mathfrak{R} = \bar{V}_{py}^{\prime 2} / \bar{V}_{fy}^{\prime 2}. \tag{17}$$

It is difficult to devise a simple but accurate mathematical model for \mathfrak{R} , particularly in an inhomogeneous turbulence field. In reality there should be a “memory effect” by which the migrating particles tend to retain the turbulence levels of earlier instants. A theoretical constitutive relation for the particle Reynolds normal stress in the presence of ‘memory effect’ is given by Shin and Lee [50].

In a practical Eulerian-type calculation, estimates of \mathfrak{R} might have to be made from local turbulence properties. This may not be very accurate, especially since the gradient of fluid turbulence near the wall is very high. In defence of a simple calculation scheme it may be noted however that (the not unsuccessful) mixing length theories of fluid turbulence employ similar assumptions. Simple theories of

homogeneous, isotropic turbulence [42] predict that for the particles to be in local equilibrium with the fluid turbulence $\mathfrak{R} = T_L/(\tau + T_L)$, where T_L is the Lagrangian time scale of fluid turbulence. Some measurements in this area are reported by Binder and Hanratty [3, 54]. Binder and Hanratty provide the following experimental correlation for \mathfrak{R} [their Eq. (18)],

$$\mathfrak{R} = \frac{1}{1 + 0.7(\tau_1/T_L)} \quad (18)$$

\mathfrak{R} varies with the wall co-ordinate as T_L varies. For very small particles $\tau_1 \rightarrow 0$, and consequently $\mathfrak{R} \rightarrow 1$. In other words, very small particles essentially follow fluid turbulence. For large particles, $\tau_1 \rightarrow \infty$, $\mathfrak{R} \rightarrow 0$. Although $\mathfrak{R} \rightarrow 0$, the product $\tau^+\mathfrak{R}$, however, remains finite in this limit and becomes independent of τ^+ . This is why neglect of the acceleration term in Eq. (15) would predict a constant deposition velocity when τ^+ is very large.

3 Simulation of fluid turbulence

For the purposes of illustration, a simple method is used here to generate the fluid turbulence field as described in Appendix 2. The mean fluid velocity, fluid rms velocity, Lagrangian time scale, diffusivity and the mean temperature profile are all expressed as functions of the wall co-ordinate y^+ . The present theory is not limited on this account. Any other suitable turbulence model for describing the fluid flow field could be used in conjunction with the present theory of particle transport.

Accurate prediction of fluid rms velocity is important. The variation of fluid rms velocity as a function of wall coordinate can be determined from measurements [4, 17, 30, 31], near-wall modeling work [7] and direct numerical simulation [29]. The particular empirical curve-fit for fluid rms velocity given in Appendix 2 is compatible to these cited works. Other equations with piecewise continuous (and differentiable) curve-fits can be used, if deemed appropriate. It is instructive to plot and study the detailed variations of $\overline{V_{iy}^2}$ and $\overline{V_{py}^2}$ with y^+ for various values of τ_1/T_L , because of the importance of such variations in understanding the nature of turbophoresis.

4 Non-dimensionalization, boundary conditions and solution methods

In Eqs. (13)–(15) all velocities are non-dimensionalized by the fluid friction velocity u_* , diffusivities are non-dimensionalized by kinematic viscosity ν , distances by (ν/u_*) , and the particle partial density by its value outside the boundary layer or at the channel centreline.

The details of how to account for the roughness of the surface has been given in Appendix 2. It is assumed that, on a rough surface, the virtual origin of the velocity profile is shifted by a distance e away from the wall [19], where $e = f(k_s)$, k_s being the effective roughness height. The particles are assumed to be captured when they reach the level of effective roughness height, i.e., at a distance b above the origin of the velocity profile, where $b = k_s - e = k_s - f(k_s)$. The data given by Grass is sparse, and more measurements (or DNS results) are needed to accurately determine the exact form of $f(k_s)$; when such an expression is available, it can easily be used with the unified advection-diffusion deposition theory. For numerical illustrations, a simple linear relation, $e = 0.55 k_s$, proposed by Wood [57] is therefore used.

Finally, the effect of ‘interception’ is accounted for by assuming that a particle is captured when its centre is at a distance r away from the effective roughness height, where r is the radius of the particle. The lower limit of integration domain is taken as $y^+ = y_0^+ = y_0 u_* / \nu$, where y_0 is given by $y_0 = b + r$. (19)

If shear-induced lift is included, then Eqs. (13), (15a) and (15b) are to be solved simultaneously to determine $\bar{\rho}_p$, \bar{V}_{px} and \bar{V}_{py} . In this paper, we have used the simplified momentum Eq. (15c) for numerical illustrations, thus only Eqs. (13) and (15c) need to be solved. For numerical solutions, an array of discrete grid points in the y -direction is created and the equations are discretized. Since Eq. (15c) is non-linear, it is robustly solved by a ‘‘time-marching technique’’ (e.g., see [14, 23, 35]) by artificially adding a pseudo time-derivative term in the equation and then marching forward in time until convergence is obtained, at which point the pseudo time-derivative term vanishes and thus the solution obtained is that of the original equation. This gives numerical values of \bar{V}_{py}^c at each grid point. Any other suitable numerical technique can be used to solve Eq. (15c), if so desired. The numerical solution procedure for Eq. (13), $\frac{d}{dy} \left\{ -(D_B + D_t) \frac{d\bar{\rho}_p}{dy} - D_T \bar{\rho}_p \frac{d \ln T}{dy} + \bar{\rho}_p \bar{V}_{py}^c \right\} = 0$, is straight-forward; one writes the equation in discretized finite-difference form at each grid point and then Gaussian or Gauss-Jordan elimination may be used to solve values of $\bar{\rho}_p$ at each grid point.

Equation (15c) is a first order, non-linear differential equation. It can be written in finite difference form and integrated with one boundary condition. [$\bar{V}_{py}^c = 0$ at the channel centreline, or, at a sufficient distance away from the wall where the gradient in turbulence intensity is negligibly small. In a boundary layer type calculation, one could specify the ‘laminar slip velocity’ at the edge of the boundary layer.] Since Eq. (15c) does not depend on particle concentration it can be solved first on its own and the

solved values of $\bar{V}_{py}^c(y)$ can then be used to solve the particle continuity equation. Equation (13) shows that $\bar{\rho}_p$ needs two boundary conditions. These are provided by specifying values of $\bar{\rho}_p$ at the channel centreline (or at a sufficient distance away from the wall) and at the lower boundary y_0 (given by Eq. 19). In most references on calculations of mass transfer or deposition, the lower boundary is taken on the solid boundary itself. Equation (19) presents a method of accounting for the effects of roughness elements in modifying the velocity profile and the capture of particles.

It is usually assumed in mass transfer calculations that the concentration at the lower boundary is zero [$\bar{\rho}_p = 0$, at $y = y_0$]. Rigorous derivations based on kinetic theory show that this boundary condition is strictly not true even in the pure diffusion limit of very small particles. In the pure inertial limit of large particles, a more appropriate condition at the lower boundary is $\partial\rho_p/\partial y = 0$. It was found, however, that, in the inertial limit, the effects of such boundary conditions on the magnitude of the calculated deposition velocity are negligible. This is because the convective velocity \bar{V}_{py}^c can be calculated from Eq. (15c) without any reference to the concentration profile, and, in the inertial limit, the deposition velocity is almost entirely controlled by \bar{V}_{py}^c . Although the deposition velocity remains unaffected, the concentration profile close to the wall does depend on the particular boundary condition employed. For a proper formulation of the boundary condition for the particle concentration at the wall one would have to resort to kinetic theory.

The particle concentration changes rapidly with distance close to the surface. One therefore needs a non-uniform computational grid for solving the particle continuity equation. The first two grids perpendicular to the solid surface should be taken very close to each other, the grid spacings towards the free stream can then vary according to a suitable geometric progression.

Once the values of $\bar{\rho}_p$ and \bar{V}_{py} are determined numerically at all grid points, including at the wall, Eq. (13) is used to calculate the particle mass transfer rate on the wall J_{wall} . The non-dimensional deposition velocity V_{dep}^+ can then be calculated from J_{wall} by the application of the Eqs. (3) and (5). It is to be remembered that, with interception, the effective wall boundary is situated at $y^+ = y_0^+ = y_0 u^*/\nu$, where y_0 is given by Eq. (19).

5 Results and discussion

5.1 Results

Most experiments and theoretical treatments on particle deposition explore the fully developed vertical flow. There

is no streamline curvature in time-mean motion of the fluid, thus inertial impaction (by which inertial particles deviate from the fluid streamlines and may hit solid boundaries) is eliminated. Gravitational settling also plays a minor role. Hence the effects of molecular and turbulent processes on deposition can be studied more effectively in this configuration. However, the particle equations given in Guha [22] automatically describe inertial impaction and gravitational settling when they are present. The experimental data compiled by McCoy and Hanratty [34] shows considerable scatter, here only Liu and Agarwal [32] data are plotted as this is generally accepted as one of the most dependable data set and to keep the discussion focused. The experiments were conducted in a glass pipe of internal diameter (D) 1.27 cm; monodispersed, spherical droplets of uranine-tagged olive oil were used (thus the deposition can be modelled without rebound), pipe Reynolds number (Re_D) was 10,000, and $\rho_p^0/\rho_f = 770$. By combining u_* calculated from the Blasius's formula, [22] has shown that $(D_B/\nu)^2/3\tau^{+1/3} = f(Re_D, D, \rho_p^0/\rho, \text{fluid properties}) = \psi$. Thus for different values of ψ , different curves of V_{dep}^+ versus τ^+ would be obtained.

Figure 2 shows the relative importance of pure diffusion and pure inertial effects in the equation for mass flux (Eq. 13). In order to isolate the effects of fluid turbulence, the flow considered is isothermal (no thermal diffusion) and all body forces (such as electrical forces) are absent. The pure diffusion case is calculated by assuming that the turbulence is homogeneous. The source term in the RHS of Eq. (15c) is zero and, consequently, the convective velocity, \bar{V}_{py}^c , is zero. Under these circumstances, Eq. (13) becomes identical with Eq. (1)—the Fick's law of diffusion. The deposition velocity monotonically decreases with increasing relaxation time. This case was calculated by taking the lower boundary at $y^+ = 0$. The behaviour of the deposition velocity, however, changes if one includes the effects of interception. The lower boundary is now given by Eq. (19). As the lower boundary is shifted, the effective resistance against mass transfer decreases. For large relaxation times, this effect can more than offset the effect of lower Brownian diffusion coefficient, D_B . For large relaxation times, the calculated deposition velocity, therefore, increases substantially with increasing relaxation time due to interception, even when the convective velocity, \bar{V}_{py}^c , is neglected [the interception effect shown in Fig. 2 is the minimum because it is shown for $k_s = 0$, i.e., $b = 0$ in Eq. (19)].

For calculating pure inertial effects, only the third term in the RHS of Eq. (13) is retained. Figure 2 shows that the convective velocity goes to zero for very small particles. Its effect on the deposition velocity has become comparable to that of pure diffusion around $\tau^+ \sim 0.2$. It then rises steeply by several order of magnitude as τ^+ increases. The total

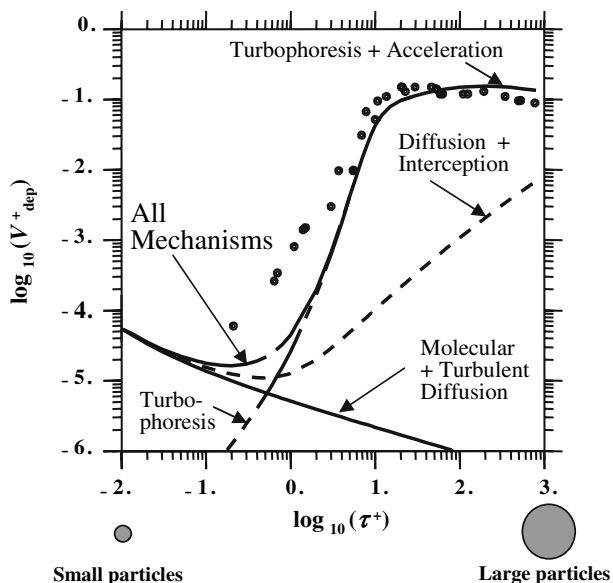


Fig. 2 Computed deposition rate versus relaxation time: Effects of pure diffusion, pure inertia and interception. Solution of Eq. (13) retaining all terms (*broken straight line*); pure diffusion: solution of Fick’s law, Eq. (1), with lower boundary at wall ($y_0^+ = 0$) (*straight line*); pure diffusion: solution of Fick’s law, Eq. (1), with interception ($y_0^+ = r^+$) (*dashes*); pure inertial deposition: solution of Eq. (13) retaining only the third term in the RHS (*double dash straight line*). For all computed curves, $k_s^+ = 0$, $\Delta T = 0$, $\zeta = 0$. Experiments [32] (*filled circle*)

deposition is calculated by retaining all terms in Eq. (13). It merges with the pure diffusion case for very small particles and merges with the pure inertial case for large particles. The relative importance of diffusion, inertia and interception can clearly be appreciated from Fig. 2.

Figure 3 shows the variation in deposition velocity with relaxation time for five different roughness parameters: $k_s^+ = 0$, $k_s^+ = 0.5$, $k_s^+ = 1$, $k_s^+ = 2$ and $k_s^+ = 4$. Equations (15c) and (13) are solved for isothermal flow (no diffusion due to temperature gradient). The calculations show that the presence of small surface roughness even in the hydraulically smooth regime significantly enhances deposition especially of small particles. Given that the deposition velocity varies by more than four orders of magnitude in the range of investigation, it is remarkable that a simple, universal equation (Eq. 13) agrees so well with measurements.

Figure 4 shows the effects of temperature gradient on the deposition velocity. [Eq. (14) shows that the thermal drift has a ‘stressphoretic’ component and a thermophoretic component.] Equations (15c) and (13) are solved for five cases: $\Delta T = 0$, $\Delta T = 5$ K, $\Delta T = 20$ K, $\Delta T = 35$ K, $\Delta T = 50$ K where ΔT is the temperature difference between the upper boundary of the calculation domain ($y^+ = 200$) and the pipe wall (the wall is cooled). Even a small temperature difference (e.g., $\Delta T = 5$ K) has a very

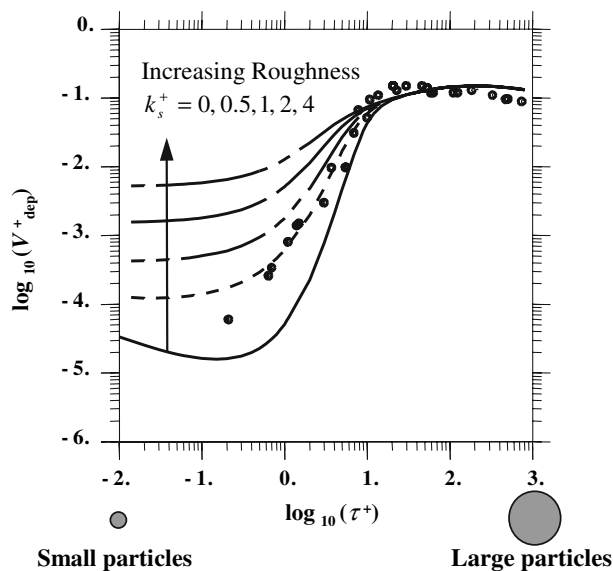


Fig. 3 Effects of surface roughness on the predicted deposition rate. $k_s^+ = 0$ (*straight line*), $k_s^+ = 0.5$ (*dashes*), $k_s^+ = 1$ (*double dash straight line*), $k_s^+ = 2$ (*broken straight line*), $k_s^+ = 4$ (*single dash straight line*). For all computed curves, $\Delta T = 0$, $\zeta = 0$, no lift force. Experiments [32] (*filled circle*)

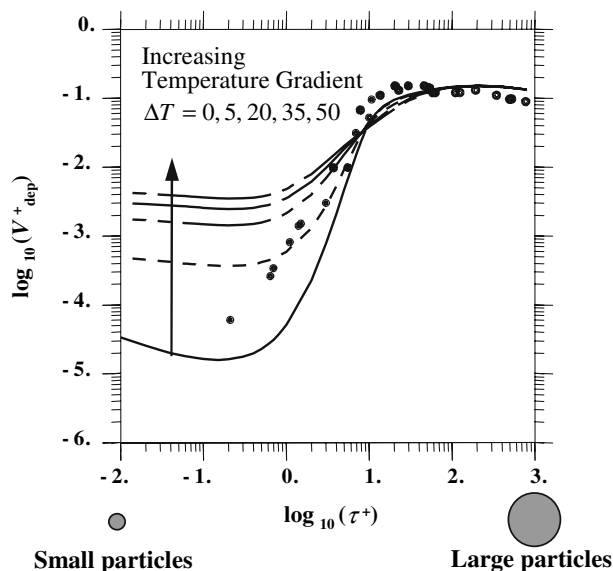


Fig. 4 Effects of thermal diffusion on the predicted deposition rate. $\Delta T = 0$ (*straight line*), $\Delta T = 5$ K (*dashes*), $\Delta T = 20$ K (*double dash straight line*), $\Delta T = 35$ K (*broken straight line*), $\Delta T = 50$ K (*single dash straight line*). For all computed curves, $k_s^+ = 0$, $\zeta = 0$, no lift force. Experiments [32] (*filled circle*)

significant effect on the deposition velocity, particularly for small particles. Considering that a modern gas turbine blade may be cooled by 300–400 K compared to the gas temperature, it is expected that thermophoresis would play an important role there. For $1 < \tau^+ < 10$, there is an interaction between thermophoresis and turbophoresis.

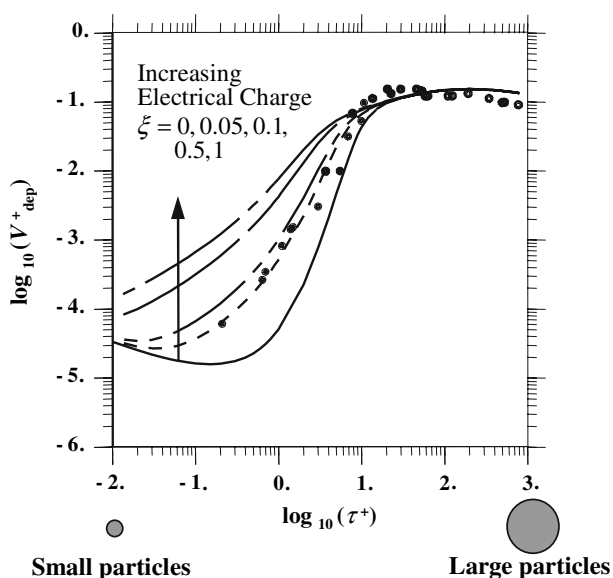


Fig. 5 Effects of electrostatic charges (mirror charging) on the predicted deposition rate. $\xi = 0$ (straight line), $\xi = 0.05$ (dashes), $\xi = 0.1$ (double dash straight line), $\xi = 0.5$ (broken straight line), $\xi = 1$ (single dash straight line). For all computed curves, $k_s^+ = 0$, $\Delta T = 0$, no lift force. Experiments [32] (filled circle)

Figure 5 shows that the electrical force due to mirror charging also has significant effect on the deposition velocity. A parametric study on the amount of charge on each particle is conducted by specifying various values ξ [see discussion following Eq. (16)]. It is interesting to note that the most significant enhancement in deposition velocity takes place approximately around $\tau^+ \sim 0.3$ where the unassisted deposition curve began to rise in Fig. 2. Of course, the effects of the electrostatic forces will be more prominent in the presence of an external electric field, the calculation of which is straightforward Eq. (16).

5.2 Discussion

The first term in the RHS of Eq. (13) is the diffusion due to a gradient in the particle concentration [same as Fick’s law given by Eq. (1)], the second term represents the diffusion due to a gradient in the temperature and the third term represents a convective contribution. Equation (15) relates the particle convective velocity with the gradient in turbulence intensity (turbophoresis) and other external forces. From Eqs. (15c) and (17), we can write the convective turbophoretic velocity ($V_{p,turbo}$) as

$$V_{p,turbo} = \tau_I \left[-\frac{\partial}{\partial y} \left(\Re \overline{V_{fy}^2} \right) \right]. \tag{20}$$

It is important to note that the turbophoretic term depends on the *particle* rms velocity, which may be different from

the fluid rms velocity if the particle inertia is large. When the particles are very small, they effectively follow the fluid eddies and the two rms velocities are essentially the same. In this limit, $\tau_1 \rightarrow 0$, Eq. (20) shows that $V_{p,turbo} \rightarrow 0$. Turbophoresis is thus negligible for small particles even if there exists a gradient in turbulence intensity. Fick’s law is, therefore, an adequate description for the deposition of small particles, in the absence of external forces. As τ_1 increases, the turbophoretic term assumes dominance, thereby increasing the deposition rate by a few order of magnitude. However, as τ_1 increases, the particles are less able to follow fluid fluctuations and the particle rms velocity becomes progressively smaller as compared to the fluid rms velocity. This is one of the factors responsible for the eventual decrease in deposition velocity with increasing particle size when τ_1 is very large. Equation (20) shows that the turbophoretic velocity also vanishes ($V_{p,turbo} = 0$), for all particles irrespective of the particle inertia, when the flow is *not* turbulent or when the turbulence is homogenous [$\partial/\partial y(\overline{V_{fy}^2}) = 0$]. However, even in laminar flow, Eqs. (13) and (15) apply, and can predict all such effects like Brownian diffusion, thermophoresis, and convective slip velocity due of streamline curvature and external body forces such as gravity or electrical interactions.

It is crucial to incorporate the particle momentum equation (Eq. 15) in the analysis. Absence of this equation in many previous analyses which solve only the particle continuity equation necessitated postulations such as the stop distance models. It is shown here (Fig. 2) that, on the other hand, deposition velocity for particles bigger than a critical size could almost be determined *from the momentum equation alone*. [The critical size is about $\tau^+ \approx 1$ when $k_s^+ = 0$ and $\Delta T = 0$ as shown in Fig. 2, but increases when thermal diffusion or roughness elements are present as shown in Figs. 3 and 4.] The first term in Eq. (15c) represents particle acceleration, the second term is the viscous drag and the third term arises from the turbulent fluctuations. When $\tau^+ \rightarrow \infty$, the viscous drag term is negligible, and the acceleration term is balanced by the turbulence term. However, in this limit, the turbulence term also tends to zero as $\Re \rightarrow 0$. As τ^+ is decreased from this limit, the turbulence term grows and so does the convective slip velocity $\overline{V_{py}^{c+}}$. The deposition velocity therefore increases with decreasing particle size in this range (Fig. 1, regime 3). This trend in deposition velocity, however, does not continue all the way to very small particles because the viscous drag term assumes importance. The viscous drag term increases with decreasing particle relaxation time, and, tries to reduce the slip velocity. The turn over point occurs around $\tau^+ = 30$. For $\tau^+ < 30$, the deposition velocity starts decreasing with decreasing relaxation time (Fig. 1, regime 2). In this regime, the acceleration term

loses importance, and the viscous term usually balances the turbulence term. However, for small particles the Brownian and turbulent diffusion of particles begin to dominate and the deposition velocity rises again with decreasing τ^+ (Fig. 1, regime 1).

It is to be noted that it is because of the acceleration term in Eq. (15c) that the deposition velocity decreases with increasing relaxation time in regime 3 of Fig. 1. If the acceleration term was not included, Eq. (15c) would have predicted a constant deposition velocity for very large relaxation times [this is a characteristic of some previous calculation schemes, even the Lagrangian calculation by Fan and Ahmadi [15] show this feature of constant deposition velocity in regime 3]. This is so because, as $\tau^+ \rightarrow \infty$ although $\Re \rightarrow 0$, the product $\tau^+\Re$, however, remains finite in this limit. Equation (17) shows that, as $\tau^+ \rightarrow \infty$, $\tau^+\Re \rightarrow 1.43T^+$.

The particle transport given by Eq. (13) has a diffusive and a convective part. The particles are transported by these two mechanisms. (The old “free flight” is effectively calculated by the present model of turbophoresis.) Very small particles complete the last part of their journey to the wall mainly by Brownian diffusion and very large particles reach the wall mainly by the convective velocity imparted by turbophoresis. For intermediate sized particles, a combination of both mechanisms is responsible.

Turbophoresis is the main mechanism which injects particles from the buffer region of a turbulent boundary layer into the region close to the wall (say, $y^+ < 20$). In this region close to the wall, $\partial J/\partial y = 0$ for fully developed flow; the total particle flux, convective plus diffusive, remains constant (i.e., whatever particle flux enters into this region must reach the wall surface to satisfy continuity and to attain a steady state). Large particles may acquire sufficient \bar{V}_{py}^c to enable them to coast to the surface—in this case $\bar{\rho}_p$ would remain approximately constant close to the wall. The convective velocity may not be sufficient for small particles to coast all the way to the surface; in order to keep the total particle flux constant to satisfy continuity, the convective flux in this case may need to be supplemented by a large diffusive flux which is achieved by the appropriate development of particle density profile close to the wall. If the predicted value of \bar{V}_{py}^c close to wall is inaccurate or the wall boundary condition for $\bar{\rho}_p$ is improper, then in order to keep J invariant close to the wall, the predicted concentration profile close to the wall would not be accurate. The inclusion of the shear-induced lift force in the particle momentum equation affects the convective velocity and particle concentration close to the wall.

For numerical illustrations here the turbulent Schmidt number is taken as unity ($D_t = \varepsilon$). Any other appropriate value may be used with the present framework. Theories show that the Schmidt number in homogenous isotropic

turbulence is close to 1 [40, 42]. Direct numerical simulation by Brooke et al. [5] showed that the Schmidt number varied across a pipe within the limits 0.6 and 1.4. The issue of determining D_t in inhomogeneous turbulent flow is complex. In the past, sometimes efforts have been made to stick to the Fick’s law and (non-physically) alter the value of particle diffusivity (for example, [33]) to obtain agreement between theoretical and experimental deposition rates. In contrast, it is assumed here (only for numerical illustrations) that the term $\bar{\rho}_p \bar{V}_{py}^c$ in equation (A2) of Appendix 1 retains the same value as in homogeneous isotropic turbulence, but that a convective particle drift arises in an inhomogeneous field by quite a different physical effect - turbophoresis. The unified advection–diffusion theory presented here thus shows that it is the Fick’s law itself that needs to be augmented in inhomogeneous turbulent flow and when other effects such as body forces are present (Eq. 13).

The effects of different particle transport mechanisms come out naturally from the present analysis in a physically satisfying manner and there is scope to add other effects in a straightforward, logical way. The present theory is also logical in finding the combined effects of different transport mechanisms, as the appropriate *forces* are added in the momentum equation and the combined “velocity” or flux is *calculated* by solving the continuity and momentum equations. This should be superior to the often-used *linear* addition of respective ‘velocities’ in order to determine the combined mass flux.

Example calculations are included here to show how particular models for various transport mechanisms can be incorporated in this general framework. For example, Eq. (11) has been used to quantify the thermophoretic force, Eq. (18) has been used for quantifying \Re , and the equations of Appendix 2 have been used to calculate the fluid turbulence field. The users can easily replace these example models with more accurate versions, if desired. Similarly any suitable boundary condition for $\bar{\rho}_p$ at the wall can be implemented. For all numerical illustrations and for comparisons with experiments and other theoretical predictions, we have considered the most explored flow configuration: vertical, fully-developed channel flow. However, the method is general and the analysis presented in Appendix 1 is also applicable for the boundary layer type flow.

The present theory offers a simple, fast and reliable computational tool of practical use to engineers. It is possible to combine the present scheme for calculating particle motion with well-established Eulerian flow solvers for calculating the flow field of the primary fluid in complex geometries (e.g., deposition of particles on internally cooled, highly curved, gas turbine blades or that of water droplets on steam turbine blades).

6 Conclusion

A unified theory of mass transfer for particles (or droplets) suspended in a fluid is presented, which can be applied to turbulent or laminar flow. The procedure consists of writing the particle continuity and momentum conservation equations and then conducting Reynolds averaging, which, for fully-developed vertical flow in channels, results in the equation set (13), (15a) and (15b). The equations are simple, and a clear physical interpretation is possible for each term.

It is crucial to incorporate the particle momentum equation (Eq. 15a–15c) in the analysis, since it computes the particle convective velocity from fundamental principles. The unified advection–diffusion theory can compute the effects of molecular and turbulent diffusion, inertial impaction, thermophoresis, turbophoresis, electrostatic forces, gravitational settling, shear-induced lift force, surface roughness and particle interception. Other transport mechanisms, if needed, can be incorporated by including the appropriate forces in the particle momentum equation (Eq. 9). The theory applies to particles of all sizes. (The particle relaxation time, Eq. (4b), includes correction for the departure from Stokesian drag regime for large particles and rarefied gas effects for very small particles.)

Calculations (Fig. 3) show that the presence of small surface roughness even in the hydraulically smooth regime significantly enhances deposition of small particles. Figure 4 shows that thermophoresis can be equally important (and should be considered, for example, in deposition calculations for internally-cooled gas turbine blades). For intermediate-size particles, there can be a strong interaction between thermophoresis and turbophoresis. Hence, in this range, how the turbophoretic term is modelled would influence the computation of enhancement of deposition due to thermophoresis. Figure 5 shows a parametric study of the effects of electrostatic forces due to mirror charging on deposition. The effects can be very significant depending on the amount of charge on each particle, and there is a strong interaction between this electrostatic effect and turbophoresis for intermediate-sized particles.

Equation (13) is a generalized mass transfer law which reduces to the Fick's law of diffusion in the limit of very small particles. Thus the study shows how the well-known and much-used Fick's law of diffusion fits into the broader context of particle transport. The paper provides a unified framework to treat various particle transport mechanisms in the form of equations such as Eqs. (13) and (15a, 15b, 15c); the framework is flexible for the user to adopt any suitable boundary conditions or any appropriate models (for the calculation of fluid turbulence, lift force, electrostatic force, thermophoretic force etc) than what has been used in this paper for illustration purposes. Equation (19)

shows a method of including the effects of surface roughness elements on the mass transfer rate, and the effect of interception alone on the rate of deposition can be appreciated from Fig. 2.

Appendix 1 Reynolds averaging of the particle continuity and momentum equations

Figure 6 shows the Cartesian co-ordinate system used. Substitute Eq. (12) in Eqs. (8) and (9) and then take time-mean of the resulting equations. We neglect the x -variation of any Reynolds stress terms and triple correlations of primed quantities. The continuity equation (Eq. 8) then becomes,

$$\frac{\partial}{\partial x} (\bar{\rho}_p \bar{V}_{px}) + \frac{\partial}{\partial y} (\bar{\rho}_p \bar{V}_{py} + \overline{\rho'_p V'_{py}}) = 0 \quad (\text{A1})$$

Equation (A1) shows that the particle mass flux in the y -direction, J , is given by

$$J = \bar{\rho}_p \bar{V}_{py} + \overline{\rho'_p V'_{py}}. \quad (\text{A2})$$

Similarly, the Reynolds-averaged momentum equations can be derived. For example, the Reynolds-averaged y -momentum equation (Eq. 9) can be written as

$$\begin{aligned} & \frac{\partial}{\partial x} (\bar{\rho}_p \bar{V}_{px} \bar{V}_{py}) + \frac{\partial}{\partial y} (\bar{\rho}_p \bar{V}_{py} \bar{V}_{py}) \\ & + \frac{\partial}{\partial y} (\bar{\rho}_p \overline{V_{py}^2}) + 2 \frac{\partial}{\partial y} (\bar{V}_{py} \overline{\rho'_p V'_{py}}) \\ & = \frac{1}{\tau_l} \left(-D_B \frac{\partial \bar{\rho}_p}{\partial y} - D_T \bar{\rho}_p \frac{\partial \ln \Gamma}{\partial y} + \bar{\rho}_p \tau_l (F_{Sy} + G_{Ey}) \right) \\ & + \bar{\rho}_p (\bar{V}_{fy} - \bar{V}_{py}) + \overline{\rho'_p V'_{fy}} - \overline{\rho'_p V'_{py}} + \bar{\rho}_p g_y \end{aligned} \quad (\text{A3})$$

where G_{Ey} is the y -component of electrostatic force per unit mass on the particles and g_y is the component of the gravitational acceleration in the y -direction. The coefficient of diffusion due to temperature gradient, D_T , is given by $D_T = D_B (1 + \eta/kT)$.

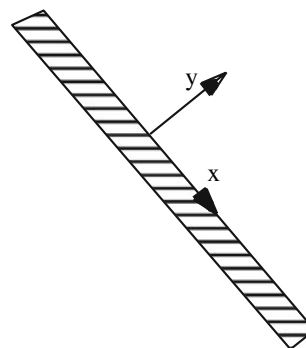


Fig. 6 Co-ordinate system used for calculation on a solid surface

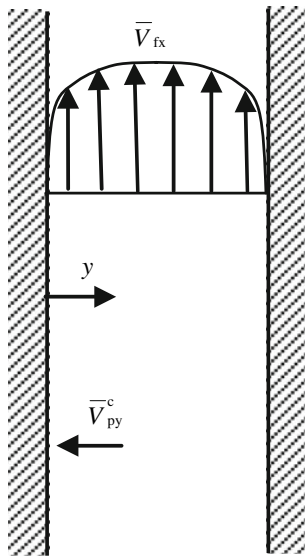


Fig. 7 Schematic for fully developed vertical upward flow

The convective velocity of the particles, \mathbf{V}_p^c , is defined by

$$\mathbf{V}_p = \mathbf{V}_p^c - (D_B \nabla(\ln \rho_p) + D_T \nabla(\ln T)) \tag{A4}$$

Consider the special case of vertical flow, i.e., the coordinate x is in the vertical direction. g then acts wholly in the x -direction and g_y is zero. For the special case of fully-developed, vertical channel flow (see Fig. 7, flow may be either in the upward or downward direction), the Reynolds-averaged continuity and momentum equations can be simplified (details given in Guha [22]) to Eqs. (13)–(15a, 15b, 15c) given in the main text.

Appendix 2 Modelling fluid turbulence

The mean motion of the fluid in the axial direction \bar{V}_{fx} and the r.m.s. fluctuation in the y -direction $\sqrt{V_{fy}^{\prime 2}}$ are expressed as functions of the wall-coordinate (y^+) as given by Kallio and Reeks [27] (with corrections of the errors in their paper).

Mean motion of the fluid in the axial direction ($V_{fx}^+ \equiv \bar{V}_{fx}/u_*$):

$$\begin{aligned} V_{fx}^+ &= y^+ && \text{for } y^+ \leq 5 \\ V_{fx}^+ &= a_0 + a_1 y^+ + a_2 y^{+2} + a_3 y^{+3} && \text{for } 5 < y^+ < 30 \\ V_{fx}^+ &= 2.5 \ln y^+ + 5.5 && \text{for } y^+ \geq 30 \end{aligned}$$

where, $a_0 = -1.076$, $a_1 = 1.445$, $a_2 = -0.04885$, $a_3 = 0.0005813$

Fluid r.m.s. velocity in the y -direction ($\sqrt{V_{fy}^{\prime 2}} = \sqrt{V_{fy}^{\prime 2}/u_*}$):

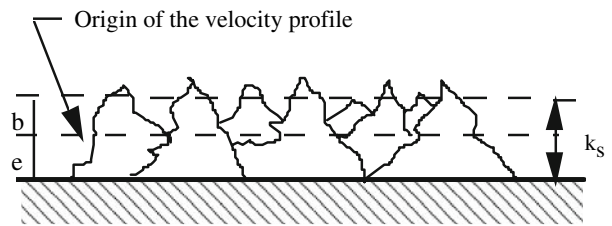


Fig. 8 Nomenclature for roughness parameters

$$\sqrt{V_{fy}^{\prime 2}} = \frac{0.005y^{+2}}{1 + 0.002923y^{+2.128}} \quad \text{for } 0 < y^+ < 200$$

Lagrangian time scale ($T_L^+ = T_L u_*^2 / \nu$):

$$T_L^+ = \frac{\varepsilon}{\nu} \left(1 / V_{fy}^{\prime 2} \right)$$

Eddy viscosity (ε): In the present work we use the universal expression of eddy viscosity valid for all y^+ , as given by Davies [13]

$$\frac{\varepsilon}{\nu} = y^{+(4-y+0.08)} \left[\frac{2.5 \times 10^7}{Re_D} \right]^{\frac{-y^+}{400+y^+}} \times 10^{-3}$$

where Re_D is the Reynolds number based on the average velocity in the pipe. For numerical illustrations here the turbulent Schmidt number is taken as unity ($D_t = \varepsilon$).

Temperature profile in the pipe [28]:

$$\begin{aligned} \frac{T - T_w}{\Delta T} &= \frac{Pr y^+}{\Delta T_{200}^+} && \text{for } y^+ < 5 \\ \frac{T - T_w}{\Delta T} &= \frac{5Pr + 5 \ln(0.2Pr y^+ + 1 - Pr)}{\Delta T_{200}^+} && \text{for } 5 \leq y^+ \leq 30 \\ \frac{T - T_w}{\Delta T} &= \frac{5Pr + 5 \ln(1 + 5Pr) + 2.5 \ln(y^+/30)}{\Delta T_{200}^+} && \text{for } 30 < y^+ < 200 \end{aligned}$$

where, $\Delta T_{200}^+ = 5Pr + 5 \ln(1 + 5Pr) + 2.5 \ln(200/30)$, T is the local temperature of the fluid, T_w is the wall temperature, Pr is the Prandtl number of the fluid and ΔT is the temperature difference between $y^+ = 200$ and the wall.

Roughness elements: It is assumed that, on a rough surface, the virtual origin of the velocity profile is shifted by a distance e away from the wall. It is further assumed that the particles are captured when they reach the level of effective roughness height, i.e. at a distance b above the origin of the velocity profile. Figure 8 schematically shows the different parameters, e.g. k_s , b and e .

References

1. Beal SK (1970) Deposition of particles in turbulent flow on channel or pipe walls. Nucl Sci Eng 40:1–11
2. Becker E (1970) Relaxation effects in gas dynamics. Aeronaut J 74:736–748
3. Binder JL, Hanratty TJ (1991) A diffusion model for droplet deposition in gas/liquid annular flow. Int J Multiphase Flow 17(1):1–11

4. Bremhorst K, Walker TB (1973) Spectral measurements of turbulent momentum transfer in fully developed pipe flow. *J Fluid Mech* 61:173–186
5. Brooke JW, Hanratty TJ, McLaughlin JB (1994) Free-flight mixing and deposition of aerosols. *Phys Fluids* 6(10):3404–3415
6. Caporaloni M, Tampieri F, Trombetti F, Vittori O (1975) Transport of particles in nonisotropic air turbulence. *J Atmos Sci* 32:565–568
7. Chapman DR, Kuhn GD (1986) The limiting behaviour of turbulence near a wall. *J Fluid Mech* 170:265–292
8. Cleaver JW, Yates B (1975) A sub layer model for the deposition of particles from a turbulent flow. *Chem Eng Sci* 30:983–992
9. Clift R, Grace JR, Weber ME (1978) Bubbles, drops and particles. Academic Press, New York
10. Crowe CT (1982) Review—numerical models for dilute gas-particle flows. *J Fluids Eng* 104:297–303
11. Cunningham E (1910) On the velocity of steady fall of spherical particles through fluid medium. *Proc R Soc Lond A* 83:357–365
12. Cussler EL (1989) Diffusion—mass transfer in fluid systems. Cambridge University Press, Cambridge
13. Davies CN (1966) Aerosol science. In: Davies CN (ed), Academic Press, London
14. Denton JD (1983) An improved time-marching method for turbomachinery flow calculation. *ASME J Eng Power* 105:514–524
15. Fan F, Ahmadi G (1993) A sublayer model for turbulent deposition of particles in vertical ducts with smooth and rough surfaces. *J Aerosol Sci* 24(1):45–64
16. Fichman M, Gutfinger C, Pnueli D (1988) A model for turbulent deposition of aerosols. *J Aerosol Sci* 19(1):123–136
17. Finnicum DS, Hanratty TJ (1985) Turbulent normal velocity fluctuations close to a wall. *Phys Fluids* 28:1654–1658
18. Friedlander SK, Johnstone HF (1957) Deposition of suspended particles from turbulent gas streams. *Ind Eng Chem* 49(7):1151–1156
19. Grass AJ (1971) Structural features of turbulent flow over smooth and rough boundaries. *J Fluid Mech* 50:233–255
20. Guha A (1994) A unified theory of aerodynamic and condensation shock waves in vapour-droplet flows with or without a carrier gas. *Phys Fluids* 6(5):1893–1913
21. Guha A (1995) Two-phase flows with phase transition, VKI lecture series 1995–06 (ISSN0377-8312). von Karman Institute for Fluid Dynamics, Belgium, pp 1–110
22. Guha A (1997) A unified Eulerian theory of turbulent deposition to smooth and rough surfaces. *J Aerosol Sci* 28(8):1517–1537
23. Guha A (1998) Computation, analysis and theory of two-phase flows. *Aeronaut J* 102(1012):71–82
24. Hesketh HE (1977) Fine particles in gaseous media. Ann Arbor Science, Ann arbor
25. Hinds WC (1999) Aerosol technology: properties, behaviour and measurement of airborne particles. Wiley, New York
26. Johansen ST (1991) The deposition of particles on vertical walls. *Int J Multiphase Flow* 17(3):355–376
27. Kallio GA, Reeks MW (1989) A numerical simulation of particle deposition in turbulent boundary layers. *Int J Multiphase Flow* 15(3):433–446
28. Kay JM, Nedderman RM (1988) Fluid mechanics and transfer processes. Cambridge University Press, Cambridge
29. Kim J, Moin P, Moser R (1987) Turbulence statistics in fully developed channel flow. *J Fluid Mech* 177:136–166
30. Kreplin HP, Eckelmann H (1979) Behaviour of the three fluctuating velocity components in the wall region of a turbulent channel flow. *Phys Fluids* 22:1233–1239
31. Laufer J (1954) The structure of turbulence in fully developed pipe flow. NACA report 1174
32. Liu BYH, Agarwal JK (1974) Experimental observation of aerosol deposition in turbulent flow. *J Aerosol Sci* 5:145–155
33. Liu BYH, Ileri TY (1974) Aerosol deposition in turbulent pipe flow. *Environ Sci Technol* 8:351–356
34. McCoy DD, Hanratty TJ (1977) Rate of deposition of droplets in annular two-phase flow. *Int J Multiphase Flow* 3:319–331
35. Mei Y, Guha A (2005) Implicit numerical simulation of transonic flow through turbine cascades on unstructured grids. *J Power Energy Proc IMechE Part A* 219(A1):35–47
36. Morsi SA, Alexander AJ (1972) An investigation of particle trajectories in two-phase flow systems. *J Fluid Mech* 55:193–208
37. Nadler B, Hollerbach U, Eisenberg, RS (2003) Dielectric boundary force and its crucial role in Gramicidin. *Phys Rev E* 68:021905–1:9
38. Ounis H, Ahmadi G, McLaughlin JB (1993) Brownian particle deposition in a directly simulated turbulent channel flow. *Phys Fluids* 5(6):1427–1432
39. Papavergos PG, Hedley AB (1984) Particle deposition behaviour from turbulent flows. *Chem Eng Res Des* 62:275–295
40. Pismen LM, Nir A (1978) On the motion of suspended particles in stationary homogeneous turbulence. *J Fluid Mech* 84:193–206
41. Ramshaw JD (1979) Brownian motion in a flowing fluid. *Phys Fluids* 22(9):1595–1601
42. Reeks MW (1977) On the dispersion of small particles suspended in an isotropic turbulent fluid. *J Fluid Mech* 83:529–546
43. Reeks MW (1983) The transport of discrete particles in inhomogeneous turbulence. *J Aerosol Sci* 14(6):729–739
44. Reeks MW (1991) On a kinetic equation for the transport of particles in turbulent flows. *Phys Fluids A* 3:446–456
45. Reeks MW (1992) On the continuum equations for dispersed particles in nonuniform flows. *Phys Fluids* 4(6):1290–1303
46. Reeks MW, Skyrme G (1976) The dependence of particle deposition velocity on particle inertia in turbulent pipe flow. *J Aerosol Sci* 7:485–495
47. Rizk MA, Elghobashi SE (1985) The motion of a spherical particle suspended in a turbulent flow near a plane wall. *Phys Fluids* 28:806–817
48. Saffman PG (1965) The lift on a small sphere in a slow shear flow. *J Fluid Mech* 22:385–400
49. Saffman PG (1968) Corrigendum to “the lift on a small sphere in a slow shear flow”. *J Fluid Mech* 31:624
50. Shin M, Lee JW (2001) Memory effect in the Eulerian particle deposition in a fully developed turbulent channel flow. *J Aerosol Sci* 32(5):675–693
51. Simonin O, Deutsch E, Minier M (1993) Eulerian prediction of the fluid-particle correlated motion in turbulent two-phase flows. *Appl Sci Res* 51:275–283
52. Soo SL (1990) Multiphase fluid dynamics. Science Press, Beijing
53. Talbot L, Cheng RK, Schefer RW, Willis DR (1980) Thermophoresis of particles in a heated boundary layer. *J Fluid Mech* 101(4):737–758
54. Vames JS, Hanratty TJ (1988) Turbulent dispersion of droplets for air flow in a pipe. *Exp Fluids* 6:94–104
55. Wang Q, Squires KD (1996) Large eddy simulation of particle-laden turbulent channel flow. *Phys Fluids* 8(5):1207–1223
56. Wells AC, Chamberlain AC (1967) Transport of small particles to vertical surfaces. *Brit J Appl Phys* 18:1793–1799
57. Wood NB (1981) A simple method for the calculation of turbulent deposition to smooth and rough surfaces. *J Aerosol Sci* 12(3):275–290
58. Zaichik LI (1999) A statistical model of particle transport and heat transfer in turbulent shear flows. *Phys Fluids* 11(6):1521–1534